Crystal Structure and Thermal Properties of $La_{1-x}Ca_xCoO_{3-\delta}$ ($0 \leq x \leq 0.4$)

Johann Mastin, Mari-Ann Einarsrud, and Tor Grande*

Department of Materials Science and Engineering, Norwegian University of Science and Technology, 7491 Trondheim, Norway

Received November 18, 2005. Revised Manuscript Received January 18, 2006

The crystal structure and thermal properties of $La_{1-x}Ca_xCoO_{3-\delta}$ have been investigated by thermogravimetrical analysis and high-temperature X-ray diffraction in air and N_2. $La_{1-x}Ca_xCoO_{3-\delta}$ is oxygen deficient at ambient temperature, and the oxygen nonstoichiometry increases with Ca content, temperature, and reducing atmosphere in line with expectations. The crystal structure of $La_{1-x}Ca_xCoO_{3-\delta}$ at ambient temperature changed from rhombohedral (hexagonal) with space group $R\bar{3}c$ for $x < 0.2$ to orthorhombic with space group $Pnma$ for $x > 0.3$. Above 200 °C the structure was rhombohedral or cubic with space group $Pm\bar{3}m$. The anisotropic thermal expansion of the lattice parameters was obtained by Rietveld refinement, and the phase transition temperature from the rhombohedral to cubic symmetry was deduced from the diffraction data. The phase transition temperature was strongly depressed by increasing the Ca content, and the findings are summarized in a phase diagram for the $La_{1-x}Ca_xCoO_{3-\delta}$ system. The second-order nature of the phase transition was discussed in terms of strain and rotation of the CoO_6 octahedra. Finally, the temperature dependence of the CaO solubility in $La_{1-x}Ca_xCoO_{3-\delta}$ was established, and isothermal phase diagrams of the pseudo-ternary system La_2O_3−CaO−CoO are presented.

Introduction

Sr and Ca substituted $LaCoO_3$ crystallize in the ABO_3 perovskite structure, where the large La^{3+} on the A site can be substituted by divalent cations such as Ca^{2+} and Sr^{2+}. Sr and Ca substituted $LaCoO_3$ have technological interests because of high mixed ionic (O^{2-}) and electronic conductivity at elevated temperatures[1,2] and are, therefore, potential materials for oxygen permeable membranes, electrodes in solid oxide fuel cells, oxidation catalysts, or oxygen sensors.[3−8]

$LaCoO_3$ remains rhombohedral up to temperatures close to the melting point; however, substitution of La^{3+} by Sr^{2+} decreases the rhombohedral distortion, and at ∼50 mol % substitution, the structure becomes cubic at ambient temperature.[9−12] It is, therefore, expected that $La_{1-x}Ca_xCoO_{3-\delta}$ and $La_{1-x}Sr_xCoO_{3-\delta}$ materials undergo a phase transition from a high-symmetry cubic phase ($Pm\bar{3}m$) at high temperature to a low-symmetry rhombohedral phase ($R\bar{3}c$) below a critical temperature, T_c, in line with similar findings for $La_{1-x}Sr_xFeO_{3-\delta}$.[13] The distortion from cubic symmetry is mainly caused by tilting of the BO_6 octahedra along one of the four diagonals in the cubic unit cell. Sr^{2+} or Ca^{2+} substitution of La^{3+} in $LaCoO_3$ is compensated by the mixed valence state of cobalt (Co^{3+}/Co^{4+}) or by creation of vacancies at the O sites. The oxygen nonstoichiometry of $La_{1-x}Sr_xCoO_{3-\delta}$ has been shown to increase with the Sr content.[11,12] The increasing oxygen deficiency due to reduction of the valence of Co has been shown to introduce chemical expansion in $La_{1-x}Sr_xCoO_{3-\delta}$.[14,15]

Kleveland et al.[16] and Faaland et al.[17] have recently demonstrated that $LaCoO_3$ and $La_{0.8}Ca_{0.2}CoO_3$ polycrystalline materials possess a nonlinear stress−strain behavior and a permanent strain after decompression. The nonlinear stress−strain behavior is related to domain reorientation of ferroelastic domains, reflecting that the cubic to rhombohedral phase transition is a paraelastic to ferroelastic transition. The phase transition results in twinning of the (100) and (110) planes of the pseudo-cubic lattice.[18,19] During compression,

* To whom correspondence should be addressed. E-mail: tor.grande@material.ntnu.no.

(1) Señarís-Rodríguez, M. A.; Goodenough J. B. *J. Solid State Chem.* **1995**, *118*, 323−336.
(2) Teraoka, Y.; Nobunaga, T.; Okamoto, K.; Miura, N.; Yamazoe, N. *Solid State Ionics* **1991**, *48* (3−4), 207−212.
(3) Ohno, Y.; Nagata, S.; Sato, H. *Solid State Ionics* **1983**, *9/10*, 1001−1008.
(4) Muller, S.; Striebel, K.; Haas, O. *Electrochim. Acta* **1994**, *39*, 1661−1668.
(5) Lindstedt, A.; Strømberg, D.; Milh, M. A. *Appl. Catal., A* **1994**, *116*, 109−126.
(6) Balachandran, U.; Dusek, J. T.; Mieville, R. L.; Poeppel, R. P.; Kleefish, M. S.; Pei, S. *J. Appl. Catal.* **1995**, *133*, 19−29.
(7) Gödickemeier, M.; Sasaki, K.; Riess, L. *Solid State Ionics* **1996**, *86/88*, 697−701.
(8) Chen, C. H.; Bouwmeester, H. J. M.; van Dorn, R. H. E.; Kruidhorf, H.; Burggraaf, A. J. *Solid State Ionics* **1997**, *98*, 7−13.
(9) Walmsley J. C.; Bardal A.; Kleveland, K.; Einarsrud, M.-A.; Grande, T. *J. Mater. Sci.* **2000**, *35*, 4251−4260.
(10) Mizusaki, J.; Mima, Y.; Yamauchi, S.; Fueki, K.; Tagawa, H. *J. Solid State Chem.* **1989**, *80*, 102−111.
(11) Mineshige, A.; Inaba, M.; Yao, T.; Ogumi, Z. *J. Solid State Chem.* **1996**, *121*, 423−429.
(12) Mastin, J.; Einarsrud, M.-A.; Grande, T. Manuscript in preparation.
(13) Fossdal, A.; Menon, M.; Wærnhus, I.; Wiik, K.; Einarsrud, M.-A.; Grande, T. *J. Am. Ceram. Soc.* **2004**, *87* (10), 1952−1958.
(14) Lein, H. L.; Wiik, K.; Grande, T. *Solid State Ionics*, in print.
(15) Chen, X. Y.; Yu, J. S.; Adler, S. B. *Chem. Mater.* **2005**, *17*, 4537−4546.
(16) Kleveland, K.; Orlovskaya, N.; Grande, T.; Moe, A. M. M.; Einarsrud, M.-A. *J. Am. Ceram. Soc.* **2001**, *84* (9), 2029−2033.
(17) Faaland, S.; Grande, T.; Einarsrud, M. A.; Vullum, P. E.; Holmestad, R. *J. Am. Ceram. Soc.* **2005**, *88* (3), 726−730.
(18) Kim, C. H.; Cho, S. Y.; Kim, I. T.; Cho, W. J.; Hong, K. S. *Mater. Res. Bull.* **2001**, *36*, 1561−1571.

10.1021/cm052547o CCC: $33.50
Published on Web 02/22/2006

energetically favorable domains remain stable and grow at the expense of less energitically favorable domain orientations. Domain reorientation has been confirmed by X-ray powder diffraction (XRD),[17,20] and energy dissipation due to domain reorientation enhances the fracture toughness of the materials. As anticipated above, the paraelastic to ferroelastic phase transition can be tailored by chemical substitution of La^{3+} by Ca^{2+}, and possibly, the ferroelastic properties of polycrystalline Sr or Ca substituted $LaCoO_3$ will be dependent on the level of substitution. So far the structural and thermal properties of Ca substituted $LaCoO_3$ have not been studied in detail. Here, we present an investigation of the chemical stability and thermal and structural properties of $La_{1-x}Ca_xCoO_{3-\delta}$. The ferroelastic to paraelastic phase transition temperature is determined, and the order parameter of the phase transition is discussed.

Experimental Section

Powder Synthesis. $La_{1-x}Ca_xCoO_{3-\delta}$ ($x = 0$, 0.1, 0.2, and 0.3) powders were prepared by solid-state reaction between La_2O_3 (Fluka, >99.98%), Co_3O_4 (Fluka, >99.995%), and $CaCO_3$ (Merck, min 99%). Dried starting materials were mixed together by ball milling in ethanol for 24 h using Si_3N_4 balls and pressed into pellets which were fired twice at 1100 °C for $x = 0$, 0.1, 0.2, and 1000 °C for $x = 0.3$ with intermediate grindings. Attempts to prepare single-phase materials with $x < 0.3$ by the solid-state method were not successful.

$La_{1-x}Ca_xCoO_{3-\delta}$ ($x = 0.4$ and 0.5) was prepared by the citrate gel method because the solid-state method resulted in a significant amount of secondary phases for these compositions. Stoichiometric solutions of the metal nitrates (Merck, min 99%) were used, and citric acid (CA; AnalaR > 99.7%) was added in the molar ratio 3/1 to that of the cations to make sure that all the cations were complexed in the solution. Ethylene glycol (EG; Acros) was further added at a molar ratio CA/EG = 1. The solution was then heated on a hot plate until a hard gel was formed. The gel was further calcined at 250 °C for 6 h. The resulting powder was ball milled in ethanol for 24 h and calcined at 900 °C for 24 h twice with an intermediate grinding. XRD patterns of the powders showed traces of CaO. Attempts to synthesize $La_{1-x}Ca_xCoO_{3-\delta}$ with $x > 0.3$ resulted in significant amounts of CaO even after long annealing at 900 °C.

The oxygen content at ambient temperature was measured by reduction of the sample in $5H_2/N_2$ at 1000 °C for 24 h. Before the reduction, the powders were annealed at 700 °C for 24 h in air and slowly cooled to ambient temperature (15 °C/h ramp) to obtain close to stoichiometric oxygen content. The temperature dependence of the oxygen nonstoichiometry was studied by thermogravimetrical analysis (Netzsch STA 449C). The powders were heated stepwise every 50−100 °C to 1000 °C with a holding time of 1−2 h. Experiments were carried out both in air and in N_2. The partial pressure of O_2 in N_2 was about 10^{-4} atm.

XRD of annealed powders was performed on a Siemens D5005 $2\theta-\theta$ diffractometer using Cu Kα radiation and a primary monochromator. The corresponding powders were also studied by high-temperature XRD (HTXRD) using a Siemens D5005 $\theta-\theta$ diffractometer using Cu Kα radiation and a secondary monochromator. The powders were dispersed in ethanol (100%) and applied on a platinum strip located in a high-temperature camera (HTK 16, Antn Paar GMbh). All measurements were performed in flowing synthetic air (99.99%) or nitrogen (99.99%, $p_{O_2} \approx 10^{-4}$ atm) atmosphere. Prior to each scan, the sample was held for 30 min at the temperature to establish equilibrium. The data were collected with a step size of 0.03° and a count time of 5−10 s to obtain a good signal-to-noise ratio.

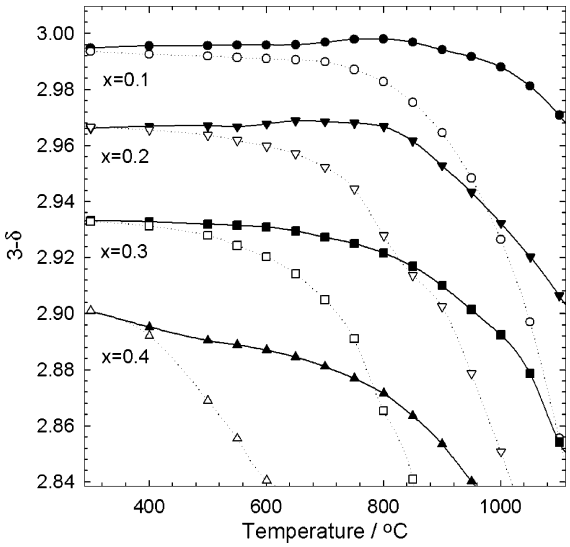

Figure 1. Oxygen nonstoichiometry of $La_{1-x}Ca_xCoO_{3-\delta}$ ($x = 0$, 0.1, 0.2, 0.3, 0.4) as a function of the temperature in air (closed symbols) and N_2 (open symbols).

The unit cell parameters were refined by the Rietveld[21] method using the program TOPAS R (Bruker AXS, version 2.1). The background was refined using a fourth-order Chebichev function. A Pearson VII function was used to refine the peak shape of both Pt and the sample. Reflections due to Pt were refined using the cubic space group $Fm\bar{3}m$. Lattice expansion of Pt was in good agreement with literature.[22] Crystal structure parameters and peak shape were finally refined simultaneously with zero point and scale. The oxygen position was also refined despite the relatively large uncertainty in the resulting position. The atomic positions for the space group are (0, 0, 1/4) for La^{3+}/Ca^{2+}, (0, 0, 0) for Co^{3+}, and (x, 0, 1/4) for O^{2-}. Below 500 °C, refinement of the isotropic temperature factor β gave inconsistency with temperature, but it had no significant influence on the refined oxygen positions. Therefore, β was fixed to 0.5 for La^{3+}, 0.24 for Ca^{2+}, 0.26 for Co^{3+}, and 0.6 for O^{2-} in agreement with data reported in the literature for similar systems.[23,24] β was refined above 500 °C and increased monotonically with temperature.

Results

Oxygen Nonstoichiometry of $La_{1-x}Ca_xCoO_{3-\delta}$. The oxygen nonstoichiometry of $La_{1-x}Ca_xCoO_{3-\delta}$ as a function of temperature is shown in Figure 1. Ca substitution results in oxygen deficiency at room temperature, which increases with the Ca content. At elevated temperatures the oxygen deficiency of $La_{1-x}Ca_xCoO_{3-\delta}$ is increasing as a result of the thermal reduction of Co. The onset temperature of the reduction is lowered by increasing the Ca substitution and by decreasing the partial pressure of oxygen.

(19) Kim, C. H.; Jang, J. W.; Cho, S. Y.; Kim, I. T.; Hong, K. S. *Physica B* **1999**, *262*, 438−443.
(20) Mastin, J.; Vullum, P. E.; Holmestad, R.; Einarsrud, M. A.; Grande, T. *Acta Mat.*, in print.
(21) Rietveld, H. M. *J. Appl. Crystallogr.* **1969**, *2*, 65.
(22) Kirby, R. K. *Int. J. Thermophys.* **1991**, *12*, 679−685.
(23) García-Muñoz, J. L.; Rodríguez-Carjaval, J.; Lacorre, P.; Torrance, J. B. *Phys. Rev.* **1992**, *46*, 4414−4425.
(24) Howard, J. C.; Kennedy, B. J. *J. Phys.: Condens. Matter* **1999**, *11*, 3229−3236.

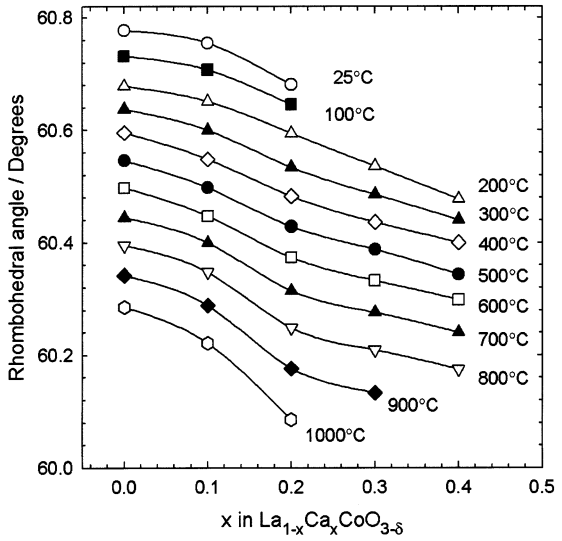

Figure 2. Rhombohedral angle of $La_{1-x}Ca_xCoO_{3-\delta}$ as a function of Ca content and temperature. Lines are guides for the eyes.

Structural Properties. The crystal structure of $La_{1-x}Ca_xCoO_{3-\delta}$ was observed to change from rhombohedral (space group $R\bar{3}c$) to orthorhombic (space group *Pnma*) with increasing Ca content at ambient temperature in line with a previous investigation.[25] $La_{1-x}Ca_xCoO_{3-\delta}$ ($x = 0$, 0.1, 0.2) was refined using $R\bar{3}c$ in the whole temperature range investigated, while $La_{1-x}Ca_xCoO_{3-\delta}$ ($x = 0.3$, 0.4) was refined using a phase mixture of orthorhombic (*Pnma*) and rhombohedral ($R\bar{3}c$) perovskite below 200 °C. At $T \geq 200$ °C, $La_{1-x}Ca_xCoO_{3-\delta}$ ($x = 0.3$, 0.4) could be refined using the space group ($R\bar{3}c$) or cubic space group ($Pm\bar{3}m$) at high temperatures.

The refinement of diffraction patterns showing evidence for the presence of two phases ($x = 0.3$, 0.4 and $T < 200$ °C) revealed an increasing amount of orthorhombic $La_{1-x}Ca_xCoO_{3-\delta}$ with increasing Ca content. This is consistent with the two-phase field of rhombohedral and orthorhombic $La_{1-x}Ca_xCoO_{3-\delta}$ reported in the region $x = 0.15-0.2$.[25] Our data show that the two-phase field extends over a relatively large composition range at ambient temperature. The transition was qualitatively confirmed by XRD down to the boiling point of N_2. The two-phase field is due to the first-order phase transition from orthorhombic to rhombohedral $La_{1-x}Ca_xCoO_{3-\delta}$.[25] A similar two-phase area has previously been reported between orthorhombic and rhombohedral $La_{1-x}Sr_xFeO_{3-\delta}$.[13] Burley et al.[25] did not report the oxygen stoichiometry of their materials, and some discrepancy due to difference in oxygen nonstoichiometry is anticipated. The orthorhombic to rhombohedral phase transition was not studied any further in this work.

The rhombohedral angle, α, of $La_{1-x}Ca_xCoO_{3-\delta}$ as a function of the Ca content and temperature is shown in Figure 2. The rhombohedral angle was calculated from the lattice parameters *a* and *c*. The rhombohedral distortion is clearly decreasing with increasing Ca content at constant temperature ($\alpha = 60°$ corresponds to the cubic perovskite). The deviation from cubic symmetry is also decreasing with increasing temperature.

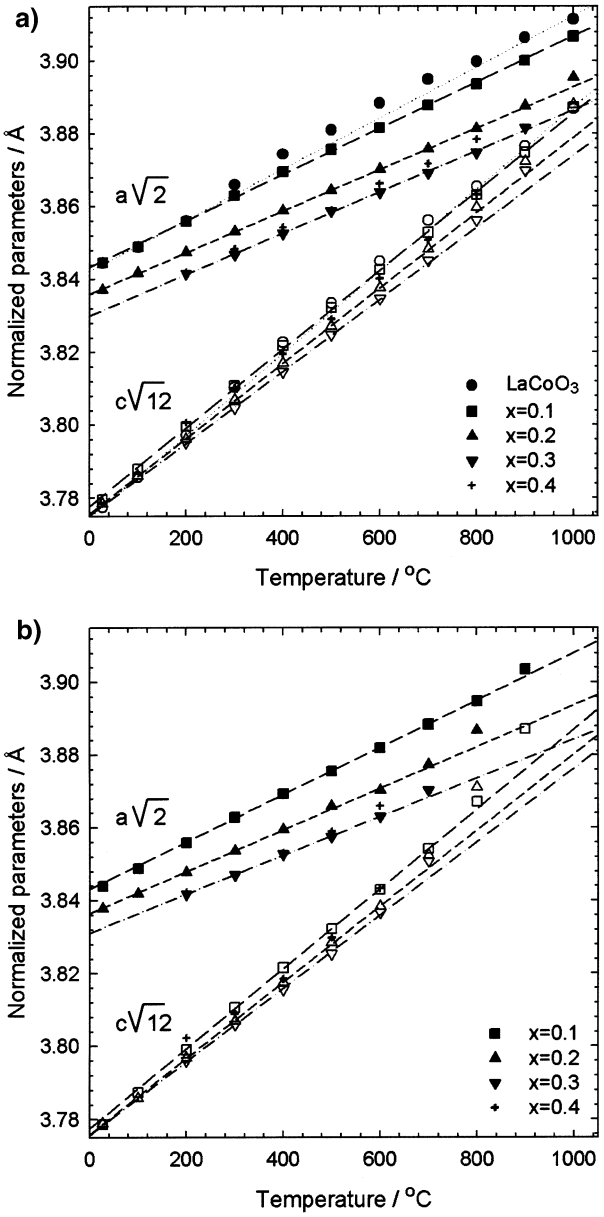

Figure 3. Normalized hexagonal lattice parameters of $La_{1-x}Ca_xCoO_{3-\delta}$ as a function of temperature (a) in air and (b) in a N_2 atmosphere. The lines in the figures are a linear fit to the data below the temperature of the onset of thermal expansion. For clarity the linear fits for $La_{0.6}Ca_{0.4}CoO_{3-\delta}$ are not included.

The normalized hexagonal lattice parameters $a/\sqrt{2}$ and $c/\sqrt{12}$ of $La_{1-x}Ca_xCoO_{3-\delta}$ are shown as a function of the temperature in Figure 3a. The distortion from cubic symmetry is evidenced by the difference between $a/\sqrt{2}$ and $c/\sqrt{12}$. The deviation from the cubic symmetry is clearly decreasing with increasing Ca content up to 30 mol %. The unit cell parameter *c* is less influenced by Ca substitution than *a*. Thermal expansion of the two lattice parameters is close to linear over a wide temperature range except for pure $LaCoO_3$, for which the thermal expansion has a nonlinear sigmoidal shape in line with data reported by Gilbu et al.[26] The linear thermal expansion coefficients (TEC) for *a* and *c*, obtained by linear fits to the data in Figure 3a, are summarized in Table 1. At high temperatures, the lattice parameters deviate

(25) Burley, J. C.; Mitchell J. F.; Short, S. *Phys. Rev.* **2004**, *B69*, 054401.

(26) Gilbu, B.; Fjellvag, H.; Kjekshus, A. *Acta Chem. Scand.* **1994**, *48* (1), 37−45.

Table 1. Linear TECs of the Lattice Parameters *a* and *c* of $La_{1-x}Ca_xCoO_{3-\delta}$ in Air and the Calculated Isotropic TEC[a]

	air (N_2)			
Ca ontent	α_a ($K^{-1} \times 10^5$)	α_c ($K^{-1} \times 10^5$)	α ($K^{-1} \times 10^5$)	temperature range (°C)
0.0	1.80	2.97	2.24	20−300; 1000
0.1	1.65 (1.71)	2.85 (2.98)	2.10 (2.15)	20−1000 (20−800)
0.2	1.49 (1.46)	2.76 (2.74)	1.93 (1.94)	20−900 (20−600)
0.3	1.45 (1.36)	2.64 (2.51)	1.88 (1.83)	200−00 (200−500)
0.4	1.54 (1.60)	2.53 (2.41)	1.95 (1.81)	200−500 (200−400)

[a] The tempearture range for each coefficient is given. Data obtained in N_2 are given in parentheses.

considerably from the linear temperature dependence, particularly at high Ca content. This deviation is due to the onset of chemical expansion due to the reduction of the valence state of Co as evidenced in Figure 1. The linear thermal expansion of *a* and *c* versus the Ca content in $La_{1-x}Ca_xCoO_{3-\delta}$ is shown in Figure 4a. A close to linear dependence of the thermal expansion of *c* with Ca content is evident, while the thermal expansion of *a* demonstrates a minimum close to $x = 0.3$. The volume of the unit cell in air as shown in Figure 4b as a function of Ca content and temperature also possesses a minimum close to $x = 0.3$.

The evolution of normalized hexagonal lattice parameters of $La_{1-x}Ca_xCoO_{3-\delta}$ in a N_2 atmosphere is shown in Figure 3b. At low temperatures the data are similar to the ones obtained in air, but they start to deviate from the linear behavior at lower temperatures because of the extensive chemical expansion of the materials at low partial pressure of oxygen. The corresponding TECs observed in N_2 are summarized in Table 1.

Phase Diagram of $La_{1-x}Ca_xCoO_{3-\delta}$. The rhombohedral to cubic phase transition temperature, T_c, derived from the HTXRD data are shown in Figure 5. To a first approximation, T_c, was determined as the intercept of the linear fit of the *a* and *c* lattice parameters in Figure 3a,b. At high temperatures the unit cell parameters deviate from a linear relationship, and the extrapolated phase transition temperatures are, therefore, clearly overestimations. This systematic deviation is illustrated in Figure 5 by arrows pointing down. At high Ca content, T_c could be determined directly from the XRD data when rhombohedral splitting of the X-ray reflections disappeared (i.e., variations in the full with at half-maximum of the reflections). In Figure 5 transition to cubic structure for $La_{0.5}Ca_{0.5}CoO_{3-\delta}$ has been included according to Faaland et al.[27]

The phase transition temperatures in the N_2 atmosphere, obtained in a similar manner, are also included in Figure 5. T_c could not be directly observed in N_2 for the compositions $x = 0.3$ or 0.4 because the materials started to decompose before the transition occurred. An estimate of the transition temperature for these two compositions is included in Figure 5.

The two-phase region due to the first-order transition between orthorhombic and rhombohedral $La_{1-x}Ca_xCoO_{3-\delta}$ is also included in Figure 5. The two-phase field is estimated

(27) Faaland, S.; Einarsrud, M. A.; Grande, T. *Chem. Mater.* **2001**, *13* (3), 723−732.

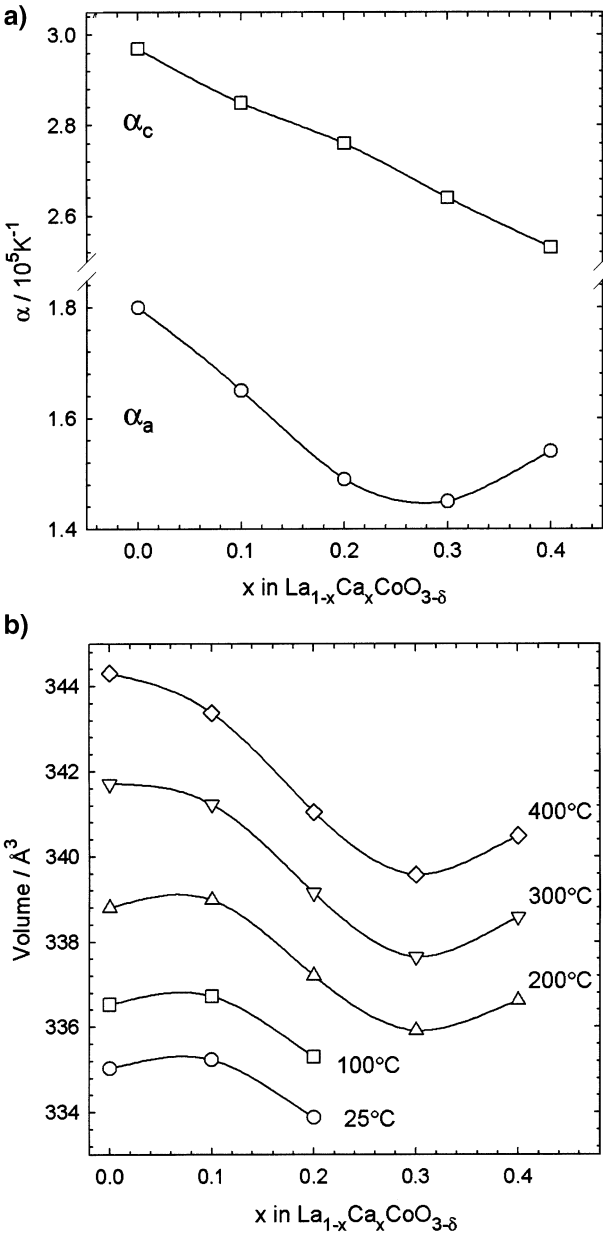

Figure 4. (a) Linear thermal expansion of the lattice parameters as a function of *x* in $La_{1-x}Ca_xCoO_{3-\delta}$ and (b) volume of the unit cell of $La_{1-x}Ca_xCoO_{3-\delta}$ as a function composition and temperature.

on the basis of the present findings and the previous report by Burley et al.[25]

Stability of $La_{1-x}Ca_xCoO_{3-\delta}$ and the Pseudo-Ternary Phase Diagram La_2O_3−CaO−CoO. All the $La_{1-x}Ca_xCoO_{3-\delta}$ materials were observed to decompose at high temperature in N_2. The phases that appeared as a result of the decomposition were La_2CoO_4 and CoO in addition to Ca depleted $La_{1-x}Ca_xCoO_{3-\delta}$. The new phases appeared at respectively 1000, 900, 800, and 700 °C for $x = 0.1$, 0.2, 0.3, and 0.4. The decomposition temperatures of the perovskite phase in N_2 are included in Figure 5. It is important to note that the phases found in equilibrium with Ca-saturated $La_{1-x}Ca_xCoO_{3-\delta}$ in air were different from the phases appearing during decomposition in the N_2 atmosphere.

Phase pure $La_{1-x}Ca_xCoO_{3-\delta}$ ($x = 0.1$, 0.2, and 0.3) was obtained by the traditional solid-state synthesis method, while $La_{0.6}Ca_{0.4}CoO_{3-\delta}$, synthesized by the citrate gel method,

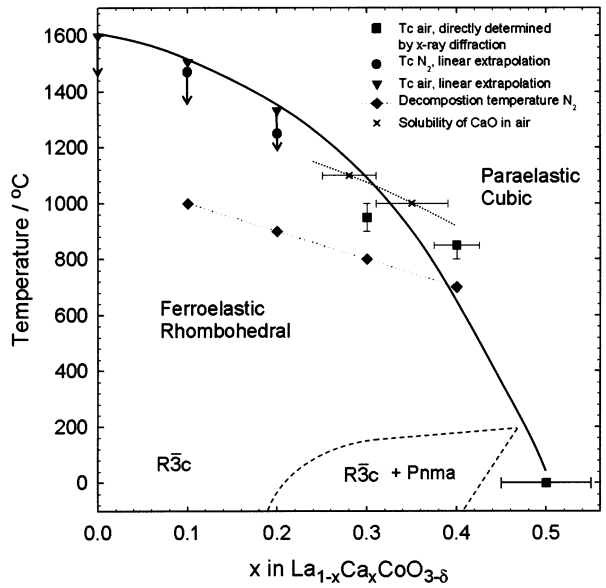

Figure 5. Phase diagram of the system $La_{1-x}Ca_xCoO_{3-\delta}$ showing the cubic and rhombohedral stability fields. The orthorhombic and rhombohedral $La_{1-x}Ca_xCoO_{3-\delta}$ two-phase field is based on the present findings and the data reported by Burley et al.[25] The temperature observed for the decomposition of $La_{1-x}Ca_xCoO_{3-\delta}$ in N_2 and the temperature dependence of the solubility limit of CaO in $La_{1-x}Ca_xCoO_{3-\delta}$ are also given in the diagram.

showed traces of CaO (<1 wt % CoO). $La_{1-x}Ca_xCoO_{3-\delta}$ ($x = 0.4$, 0.5) synthesized by the solid-state method at 1000 and 1100 °C showed clear evidence of limited CaO solubility in $La_{1-x}Ca_xCoO_{3-\delta}$. The two phases, CaO(ss) and CoO(ss), were observed coexisting with $La_{1-x}Ca_xCoO_{3-\delta}$ in a solid-state sample with nominal composition $La_{0.6}Ca_{0.4}CoO_3$ heat treated at 1100 °C. The CaO content in the perovskite was determined by quantitative Rietveld refinement, and the Ca solubility limit was found to be $x = 0.28 \pm 0.03$. The refined cell parameter of CaO(ss) showed that the solid solution between CaO and CoO at 1100 °C is in reasonable agreement with data from the reported CaO−CoO phase diagram.[28] CoO was observed to oxidize to Co_3O_4 during cooling. The estimated solid solutions along the pseudo-binary system CaO−CoO were 6 mol % CoO in CaO(ss) and 16 mol % CaO in CoO(ss). Two other coexisting phases with CaO-saturated $La_{1-x}Ca_xCoO_{3-\delta}$ were observed at 1000 °C. These two phases were $Ca_3Co_2O_6$ and a previously not reported phase. The unknown phase has a high CoO content according to a simple mass balance analysis. The decomposition temperature of $Ca_3Co_2O_6$ has been reported to be 1026 °C,[28] and it is, therefore, reasonable that the phase did not appear at 1100 °C. The CaO solubility limit in $La_{1-x}Ca_xCoO_{3-\delta}$ at 1000 °C was estimated to be $x = 0.35 \pm 0.04$. The isothermal sections of the CaO−CoO−La_2O_3 system at 1100 and 1000 °C are shown in Figure 6.

Discussion

Defect Chemistry and Thermal and Chemical Expansion. At low temperatures the substitution of La^{3+} by Ca^{2+} results in the oxidation of Co^{3+} to Co^{4+}. The relationship

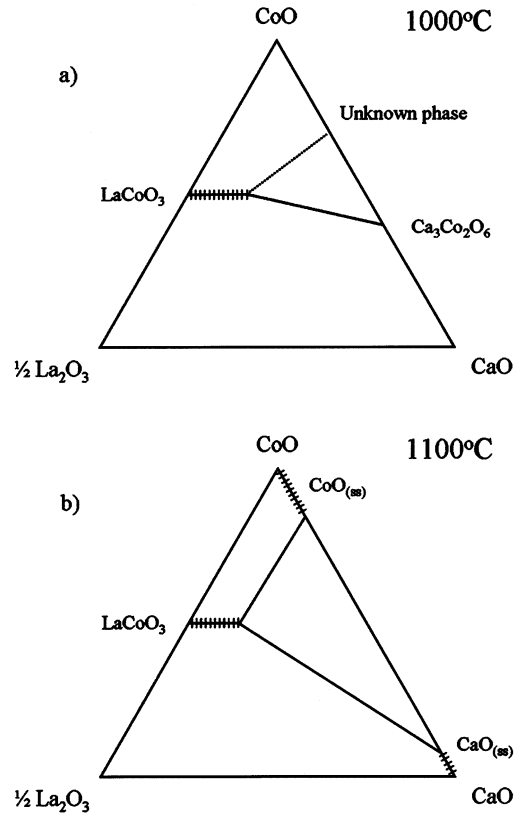

Figure 6. Isothermal sections of the ternary phase diagram of the system La_2O_3−CaO−CoO in air at (a) 1000 °C and (b) 1100 °C.

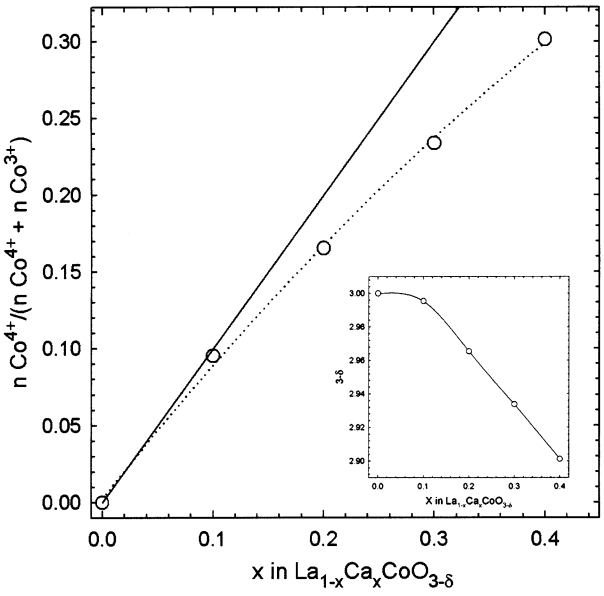

Figure 7. Fraction of Co^{4+} as a function of x in $La_{1-x}Ca_xCoO_{3-\delta}$. The solid line shows the evolution of the fraction for stoichiometric ($\delta = 0$) materials. Inset: The oxygen nonstoichiometry as function of x in $La_{1-x}Ca_xCoO_{3-\delta}$ at ambient temperature.

between the Ca content and the content of Co^{4+} at ambient temperature does not follow the predicted linear relationship (Figure 7) as a result of onset of oxygen deficiency. For $x = 0.1$ in $La_{1-x}Ca_xCoO_{3-\delta}$, the oxygen vacancy concentration is negligible. For $x > 0.1$, the oxygen nonstoichiometry is increasing almost linearly with x in $La_{1-x}Ca_xCoO_{3-\delta}$. A similar relationship has been observed for Sr substituted $LaCoO_3$.[1,29,30] At elevated temperature the oxygen nonstoichiometry of $La_{1-x}Ca_xCoO_{3-\delta}$ is increasing, as shown in

(28) Woermann, E.; Muan, A. *J. Inorg. Nucl. Chem.* **1970**, *32*, 1455−1459.

Figure 1, as a result of the thermal reduction of the valence state of cobalt

$$La_{1-x}Ca_xCoO_{3-\delta} \rightarrow La_{1-x}Ca_xCoO_{3-\delta'} + (\delta-\delta')/2O_2(g) \quad (1)$$

As shown previously for $La_{1-x}Sr_xCoO_{3-\delta}$,[1,29,30] the oxygen nonstoichiometry of $La_{1-x}Ca_xCoO_{3-\delta}$ does not saturate near $\delta = x/2$ corresponding to only Co^{3+}. For $La_{1-x}Sr_xCoO_{3-\delta}$, Petrov et al.[31] have observed that the amount of Co^{4+} increases with the Sr^{2+} content up to $x = 0.4$ and then decreases for higher Sr content. The thermal reduction goes beyond $\delta = x/2$ leading to the formation of Co^{2+}. The defect chemistry of $La_{1-x}Ca_xCoO_{3-\delta}$ and $La_{1-x}Sr_xCoO_{3-\delta}$ can be rationalized by the delocalized nature of the electrons in $LaCoO_3$ materials as shown by Lankhorst et al.[32] The defect chemistry of Sr substituted $LaFeO_3$, where the electrons are localized in a narrow electron band, displays different behavior.[33] Here the oxygen deficiency saturates at $\delta = x/2$ where x is equal to the Sr substitution.

Below the onset of thermal reduction, the thermal expansion of $La_{1-x}Ca_xCoO_{3-\delta}$ is nearly linear with temperature. For $LaCoO_3$, magnetic transition causes some deviation from linear behavior as shown previously by Gilbu et al.,[26] and Radaelli and Cheong[34] but this effect becomes less pronounced with increasing Ca substitution. However, the change in the magnetic state of $La_{1-x}Ca_xCoO_{3-\delta}$ results in a higher thermal expansion relative to other $LaMO_3$ (M = Fe,[13] Cr,[26] Mn,[35] and Ni[36]) perovskites. The decreasing thermal expansion with increasing Ca content (Figure 4a) can be inferred as an evidence for stabilizing the spin state of Co by Ca doping.

At elevated temperatures the thermal reduction of $La_{1-x}Ca_xCoO_{3-\delta}$ gives an additional contribution to the expansion due to chemical expansion. Chemical expansion of $La_{1-x}Sr_xCoO_{3-\delta}$ has recently been studied in detail by Chen et al.[15] and Lein et al.[14] The chemical expansion reported for $La_{1-x}Ca_xCoO_{3-\delta}$ is comparable to the chemical expansion of $La_{1-x}Sr_xCoO_{3-\delta}$; however, chemical expansion is shifted to lower temperatures. The reason for this is that Ca has a lower ability to stabilize Co^{4+} compared to Sr, rationalized by the lower basicity of CaO relative to SrO.

The TECs of *a* and *c* show a different dependence with increasing Ca content (see Figure 4a) which can also be related to chemical expansion and probably also some ordering of the oxygen vacancies. Ordering of the oxygen vacancies in $La_{1-x}Sr_xCoO_{3-\delta}$ has previously been reported.[37] Because the rhombohedral distortion from cubic symmetry causes a compression of the structure along the *c* axis, it is reasonable that the effect of the oxygen deficiency is most pronounced along the *a* axis as shown in Figure 4a.

Phase Stability of $La_{1-x}Ca_xCoO_{3-\delta}$. The low CaO solubility in $LaCoO_3$ relative to the corresponding solubility of SrO in $LaCoO_3$ can be rationalized by the concept of basicity. The solid solution from pure $LaCoO_3$ to pure $SrCoO_{3-\delta}$[38] is known to be stable, while $CaCoO_{3-\delta}$ has not been reported as a stable phase, which is in line with the limited solid solubility of CaO in $LaCoO_3$ reported here. SrO has a higher ability to stabilize a high oxidation state of Co compared to CaO. Similar arguments have been used to explain the significantly more exothermic enthalpy of formation from the oxides of Sr substituted $LaMnO_3$ compared to Ca substituted $LaMnO_3$.[39]

As shown in this work, single-phase $La_{1-x}Ca_xCoO_{3-\delta}$ decomposes during heating in an inert atmosphere. It is interesting to note that the phases formed as a result of the decomposition were not the same phases observed coexisting with $La_{1-x}Ca_xCoO_{3-\delta}$ in air at higher temperatures (Figure 6). It is, therefore, likely that the phases observed after decomposition do not represent a true equilibrium in the system. The decomposition reaction is more likely a metastable phase composition, and the true stability of $La_{1-x}Ca_xCoO_{3-\delta}$ in an inert atmosphere is lower than that observed by the present HTXRD investigation.

Structural Properties. Deviation from cubic symmetry at room temperature may be analyzed in terms of the Goldschmidt tolerance factor. The tolerance factor of $La_{1-x}Ca_xCoO_{3-\delta}$ shows a marginal increase with increasing Ca content from 0.987 for $LaCoO_3$ to 0.990 for $La_{0.6}Ca_{0.4}CoO_3$. Here, the coordination number (CN) for La^{3+} and Ca^{2+} is set to 12, and the CN for Co^{3+} and Co^{4+} is set to 6 neglecting oxygen deficiency. As demonstrated by Asai et al.,[40] at ambient temperature, Co^{3+} is assumed to be in the intermediate spin state and the ionic radius of Co^{3+} is assumed to be the average radius between the low spin state (0.545 Å) and the high spin state (0.61 Å). The tolerance factor increases marginally as a result of the relatively larger radius difference between Co^{4+} (0.53 Å) and Co^{3+} (~0.57 Å) compared to the small difference between La^{3+} (1.36 Å) and Ca^{2+} (1.34 Å).[41] The decreasing rhombohedral distortion at constant temperature as shown in Figure 2 is in accordance with the increasing tolerance factor. The stabilization of the orthorhombic polymorph as shown in Figure 5 cannot be rationalized by the tolerance factor and is possibly related to the magnetic state of Co. The formation of orthorhombic $La_{1-x}Ca_xCoO_{3-\delta}$, inferring a decreasing tolerance factor, points to stabilization of a intermediate or high spin state of Co with increasing Ca content as argued also from the TEC (Table 1).

(29) Mizusaki, J.; Yasuo, M.; Yamauchi, S.; Fueki, K.; Tagawa, H. *J. Solid State Chem.* **1989**, *80*, 102−111.
(30) Mineshige, A.; Inaba, M.; Yao, T.; Ogumi, Z.; Kikuchi, K.; Kawase, M. *J. Solid State Chem.* **1996**, *121*, 423−429.
(31) Petrov, A. N.; Kononchuck, O. F.; Andreev, A. V.; Cherepanov, V. A.; Kofstad, P. *Solid State Ionics* **1995**, *80*, 189−199.
(32) Lankhorst, M. H. R.; Bouwmeester, H. J. M.; Verwejj, H. *J. Solid State Chem.* **1997**, *133*, 555−567.
(33) Bahteeva, J. A.; Leonidov, I. A.; Patrakeev, M. V.; Mitberg, E. B.; Kozhevnikov, V. L.; Poeppelmeier, K. R. *J. Solid State Electrochem.* **2004**, *8*, 578−584.
(34) Radaelli, P. G.; Cheong, S. W. *Phys. Rev.* **2002**, *B66*, 094408.
(35) Hammouche, A.; Siebert, E.; Hammou, A. *Mater. Res. Bull.* **1989**, *24*, 367−380.
(36) Obayashi, H.; Kudo, T. *Jpn. J. Appl. Phys.* **1974**, *14* (3), 330−335.
(37) Kruidhof, H.; Bouwmeester, H. J. M.; van Dorn, R. H. E.; Burgraaf, A. J. *Solid State Ionics* **1993**, *63*−*65*, 816−822.
(38) Vashook, V. V.; Zinkevich, M. V.; Ullmann, H.; Paulsen, J.; Trofimenko, N.; Teske, K. *Solid State Ionics* **1997**, *99*, 23−32.
(39) Rørmark, L.; Stølen, S.; Wiik, K.; Grande, T. *J. Solid State Chem.* **2002**, *163*, 186−193.
(40) Asai, K.; Yoneda, A.; Yokokura, O.; Tranquada, J. M.; Shirane, G.; Kohn, K. *J. Phys. Soc. Jpn.* **1998**, *67* (1), 290−296.
(41) Shannon, R. D. *Acta Crystallogr.* **1976**, *A32*, 751−767.

At low Ca content the molar volume is decreasing with increasing Ca content because of the stabilization of the intermediate spin state of Co. At high Ca substitution levels the oxygen deficiency becomes dominant as indicated by the increase in the molar volume for $x > 0.3$ shown in Figure 4b. At high a Ca substitution level, the creation of oxygen vacancies in the lattice increases the molar volume and, as shown in Figure 2, the crystal structure is driven toward the cubic perovskite structure.

Figure 3a,b evidences that the lattice parameter a is more influenced by the Ca substitution than c. This variation can be understood from the octahedral rotation angle around the 3-fold axis and the octahedral strain parameter. Following a similar consideration as Howard and Kennedy[24] on $LaGaO_3$, which has the same rhombohedral structure above 150 °C, the rotation angle and strain parameter can be calculated from the refined atomic position of oxygen. For the $R\bar{3}c$ space group the oxygen position is (x, 0, $^1/_4$) and $x = {}^1/_2 + u$, with the Co atom at the origin. The angle of rotation ϕ of the octahedra is given by[24]

$$\tan \phi = 2u\sqrt{3} \tag{2}$$

The angle ϕ is 0 for the cubic perovskite. The evolution of ϕ as a function of temperature for different Ca contents in $La_{1-x}Ca_xCoO_{3-\delta}$ is shown in Figure 8a. Scattering of the data is due to the significant uncertainty in the oxygen position. Despite the uncertainty, the data demonstrate that, at constant temperature, ϕ decreases from 10.8 for $LaCoO_3$ to 9.2 for $La_{0.9}Ca_{0.1}CoO_{3-\delta}$. For a higher substitution level, ϕ is increasing and becomes for $La_{0.6}Ca_{0.4}CoO_{3-\delta}$ almost equal to the value obtained for $LaCoO_3$. We believe the increasing ϕ at high Ca content at constant temperature is caused by the increasing oxygen deficiency.

At low temperature, the rotation angle decreases almost linearly with temperature, while for higher temperatures, ϕ starts to decrease rapidly toward 0. The onset temperature for the nonlinear relationship is decreasing with increasing Ca content. The linear decrease of ϕ with temperature can be explained by increasing contribution due to vibrations. At high temperature the increasing concentration of oxygen vacancies contribute to drive the structure toward the cubic phase.

In the rhombohedral perovskites with tilted octahedra, the octahedral strain parameter, η, can be calculated by[24]

$$\eta = c \cos \phi / a\sqrt{6} \tag{3}$$

Evolution of η with temperature for $La_{1-x}Ca_xCoO_{3-\delta}$ is included in Figure 8b. $\eta < 1$ means that the oxygen octahedra are compressed along the threefold axis and evolve toward the cubic structure at high temperatures when it increases toward unity. At low temperature, η increases for $x = 0.1$ but remains constant for $x = 0.2$, 0.3, and 0.4. The strain parameter increases almost linearly with temperature. At high temperature, η starts to deviate from the linear relationship and increases rapidly toward $\eta = 1$. Increasing the Ca content in the material decreases the onset temperature for the nonlinear behavior.

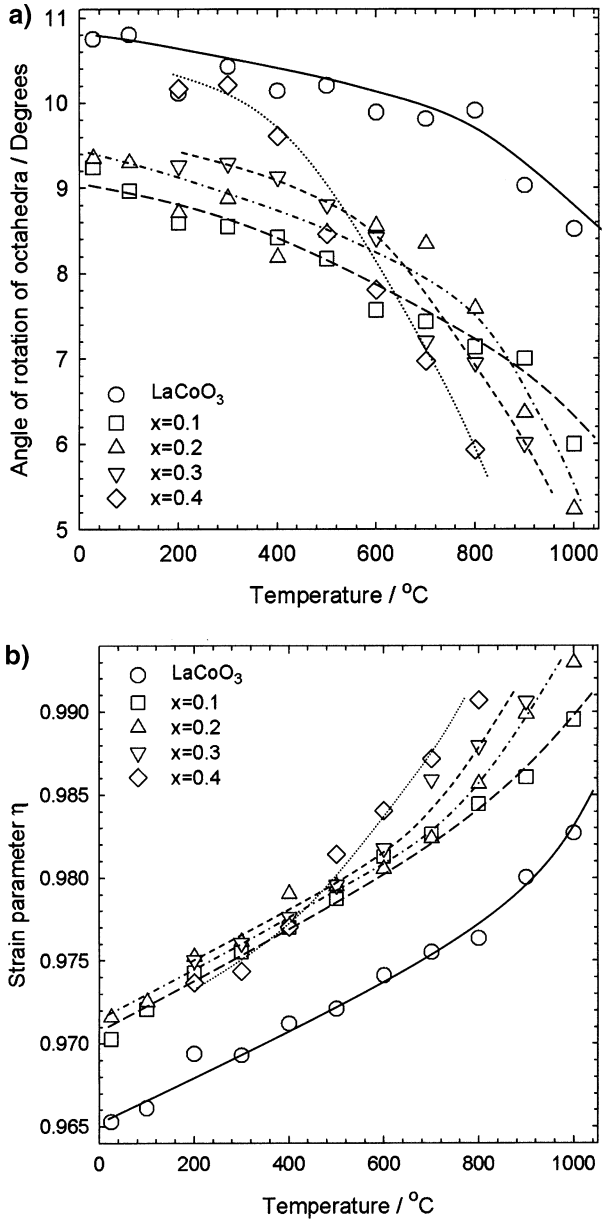

Figure 8. (a) Angle of rotation of the CoO_6 octahedra in $La_{1-x}Ca_xCoO_{3-\delta}$ and (b) octahedral strain parameter as a function of the temperature and composition. The lines are guides for the eyes.

Both parameters, η and ϕ, are in the rhombohedral structure geometrically independent but can be related. According to Thomas,[42] who has studied the relationship between lattice strain, octahedral tilt angle and octahedral strain in rhombohedral perovskites, a tilting of the octahedra leads to a contraction of the hexagonal a axis when the c axis remains unaffected. In $La_{1-x}Ca_xCoO_{3-\delta}$, the decrease of a with increasing Ca content and c, which is less influenced, are in agreement with this geometrical description.

The study of similar rhombohedral perovskites such as $LaAlO_3$[43] and $LaGaO_3$[24] has shown a similar dependency of the phase transition temperature with the angle of rotation of the octahedra and the octahedral strain parameter. The

(42) Thomas, N. W. *Acta Crystallgr*. **1996**, *B52*, 954−960.
(43) Howard, C. J.; Kennedy, B. J.; Chakoumakos, B. C. *J. Phys.: Condens. Matter* **2000**, *12*, 349−365.

rotation angle of the octahedra can be treated as the order parameter of the paraelastic to ferroelastic phase transition. The average value, $\langle\phi\rangle$, is continuously decreasing with increasing temperature and vanishes over T_c as described by the mean-field theory for a second- or higher-order phase transition.[44] Howard et al.[43] have suggested that the transition temperature was mainly dependent on the rotation angle in line with the present finding. Further studies of the ferroelastic properties of $La_{1-x}Ca_xCoO_{3-\delta}$ ceramics and related materials as a function of composition and critical temperature for the ferroelastic to paraelastic transition temperature are in progress.

Conclusion

The thermal evolution of oxygen deficiency of $La_{1-x}Ca_xCoO_{3-\delta}$ has shown that CaO has a limited ability to stabilize a high oxidation state of Co and increasing Ca substitution of $La_{1-x}Ca_xCoO_{3-\delta}$ leads to enhanced oxygen deficiency. The crystal structure of $La_{1-x}Ca_xCoO_{3-\delta}$ at ambient temperature was shown to change from a rhombohedral to an orthorhombic perovskite structure with increasing Ca substitution. The compositional dependence of the second-order rhombohedral to cubic phase transition temperature has been established by HTXRD, and the phase diagram of the $La_{1-x}Ca_xCoO_{3-\delta}$ system is reported. The order parameter of the para- to ferroelastic phase transition is shown to be related to the angle of rotation of the CoO_6 octahedra. Finally, the CaO solubility and thermal stability of $La_{1-x}Ca_xCoO_{3-\delta}$ have been determined.

CM052547O

(44) Salje, E. K. H. *Phase transitions in ferroelastic and co-elastic crystals*; Cambridge University Press: New York, 1990.